A Fault Diagnosis Method for On Load Tap Changer of Aerospace Power Grid Based on the Current Detection

ZHENHUA LI[1], QIUHUI LI[1], ZHENGTIAN WU[2], JIE YU[1], AND RONGHAO ZHENG[3]

[1]College of Electrical Engineering and New Energy, China Three Gorges University, Yichang 443002, China
[2]School of Electronic and Information Engineering, Suzhou University of Science and Technology, Suzhou 215009, China
[3]College of Electrical Engineering, Zhejiang University, Hangzhou 310027, China

Corresponding author: Zhengtian Wu (wzht8@mail.usts.edu.cn)

ABSTRACT As one of the key components of aerospace power grid, the performance of on load tap changer (OLTC) of power transformer is very important. So it is necessary to realize real-time monitoring of its status. At present, there is no feasible monitoring scheme to carry out on-line monitoring and fault diagnosis for detecting faults of OLTC. The current waveform of the switching process will be abnormal due to the contact fault, the transition resistance fault, and most of the mechanical faults. This paper presents a fault diagnosis method for OLTC based on the current detection in the process of switching. Through on-line acquisition of current waveform in the switching process, empirical mode decomposition and Hilbert–Huang transform is used to calculate normalized time-frequency spectrum, and extract fault characteristic quantity, which can realize the comprehensive diagnosis of the running state of the equipment, and identify the early fault characteristics, and promote the process of the OLTC's maintenance, from regular test to condition based maintenance. Experiment results prove that the designed fault diagnosis instrument can effectively monitor the working condition of OLTC during the switching process and make effective fault diagnosis.

INDEX TERMS On load tap changer, fault diagnosis, EMD-HHT, square Rogowski coil, current of switching process.

I. INTRODUCTION

The stability of the power grid is the guarantee of normal operation of the space launch site and aerospace engineering. As a key part of the power grid, power transformer is required to determine the running status of each component through status monitoring. This will be able to identify early signs of failure and take appropriate measures to avoid further deterioration [1]–[6]. On load tap changer (OLTC) is the only moving part in power transformer under high voltage and heavy current [7]–[9]. Due to its complex structure and high requirements of the electrical performance, its failure rate is high, which accounts for more than 20% of all transformer failures [10]–[13]. So it is urgent to monitor the running status and carry out on-line diagnose, and then take preventive measures to avoid accidents [14]–[18].

However, because of the complex mechanical structure and electrical structure of the OLTC, the faults have the character of variety. Serious faults often occur in the contact terminals and transition circuit. But the contact terminals are located inside the switch, and the OLTC is installed inside the power transformer which is located on the high voltage side. So it is difficult to monitor the status directly. Therefore, there is no effective solution for on-line monitoring and fault diagnosis of OLTC at present.

References [19] and [20] present on-line fault diagnosis methods based on acoustic emission, which records the mechanical wear by acoustic analysis [19], [20]. References [21] and [22] propose the fault detection for linear discrete time-varying systems and give a new idea [21], [22]. References [23]–[25] propose the method that by collecting the vibration signal, and using HHT (Hilbert-Huang Transform) or wavelet analysis of vibration signals to diagnose mechanical fault of OLTC [23]–[25]. The above methods are mainly used for vitro monitoring, which adopt the

mathematical algorithm to analyze failure signals. For electrical faults without obvious mechanical vibration, such as contact terminals fault and contact resistance anomaly, it is very hard to diagnose. References [26] and [27] give a sliding mode technique and can be used for the fault diagnosis of OLTC [26], [27]. Reference [28] gives a feature extraction method based on variational mode decomposition and weight divergence to improve the intelligent diagnosis level of OLTC's mechanical condition, and [29] gives a fault diagnosis method in converter transformer based on time–frequency vibration analysis, but these methods cannot monitor the electric condition [28], [29].

A fault diagnosis method for OLTC based on the current detection in the switching process is proposed in this paper. The current waveform of the fixed contact terminal of the switch can reflect the switching process. It contains rich information, such as the electric arc caused by loose contact and contact ablation, the change of current caused by transition resistance failure and other faults, time changes or other fault waveforms caused by mechanical anomalies of the switches. A more comprehensive fault diagnosis for OLTC can be done by analyzing the characteristics of the fault waveforms.

In this paper, a current sensor with a wideband and large dynamic range is used to collect real time current waveform of OLTC, and optical fiber is adopted to transmit data and realize electrical isolation between the high voltage side and low voltage side. An improved EMD-HHT (Empirical Mode Decomposition method and Hilbert-Huang Transform) algorithm is used to analyze the waveform data, and extract the fault feature quantity compared with normal switching characteristics, so as to achieve the comprehensive diagnosis of the running status of OLTC. It will be propitious to identify the early signs of faults and provide the basis for the equipment maintenance and adjustment of operation mode.

II. PRINCIPLE AND STRUCTURE

The faults of OLTC are mainly the contact terminals fault, transition resistance fault and mechanical fault. Most of the faults will cause abnormal switching current waveform, however, as the fixed contact terminals of switching are located at the high voltage side and inside the OLTC, it is difficult to monitor directly. By designing a small and well insulated signal acquisition system to collect data, the OLTC fault diagnosis method proposed in this paper can monitor the current during handover process for a running OLTC. The schematic diagram is shown in Fig.1.

Take phase A as the example, the signal acquisition system is located on the high voltage side, and the power supply module of the master sensor receives the outputs of CTI and CTII, and then converts the outputs to DC power supply for the signal conversion circuit. The signal conversion circuit collects the current waveforms of fixed contacts I and II, respectively. After signal conditioning and anti-aliasing filtering, the analog signal is converted to digital signal through a high precision A/D sampling circuit, and then transmitted to the data merging device through optical fiber after encoding.
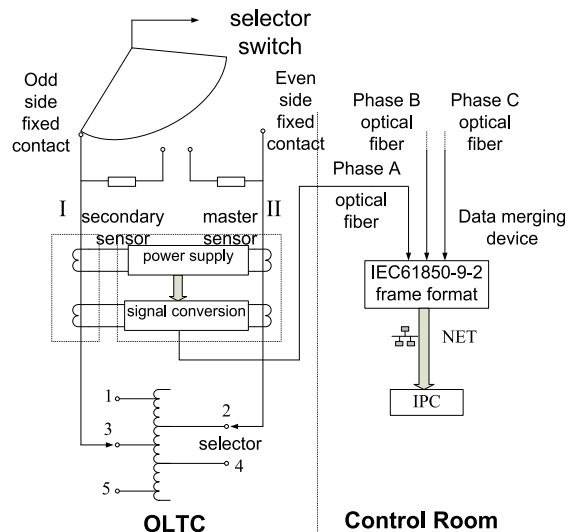

FIGURE 1. Fault diagnosis system for OLTC.

The master sensor and secondary sensor are in equipotential, and they are insulated from line I and II by using a polytef insulating sleeve. So the acquisition of current signal in the switching process can be conducted normally without affecting the safe operation of OLTC and power transformer, by using the insulation methods.

The data merging device receives the signals from phase A, B and C, which transmitted through optical fibers. After decoding, the signals are sent to the computer with a frame format of IEC61850-9-2 communication protocol. HHT time-frequency analysis is carried out by the fault diagnosis software in the computer, and the statistic feature of the current signal is extracted. At last, early signs of the faults can be identified and judgment data for the equipment maintenance and adjustment of operation mode can be provided.

III. DESIGN

The key technology of the OLTC fault diagnosis system is that the signal acquisition system can obtain energy from the power line and collect current signals, and the fault diagnosis software can identify the fault characteristics from current waveforms. Among which, the current sensor, the power supply circuit, the EMD-HHT algorithm and the diagnostic software are discussed and detailed designed as follows:

A. CURRENT SENSOR

A wide dynamic range and wide band current sensor is needed to capture the dynamic current signal during the switching process. Traditional large current sensor usually adopts a ferromagnetic current transformer. Since the current transformer with iron core is easy to be saturated when the primary current contains DC component, and the frequency band is narrow which leads to signal distortion, it is not suitable for the current measurement in this system [30]–[32]. Rogowski coil has many advantages, such as
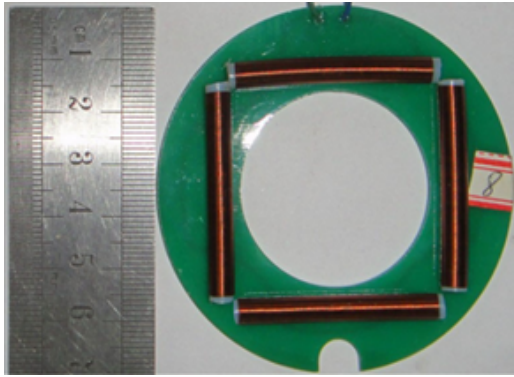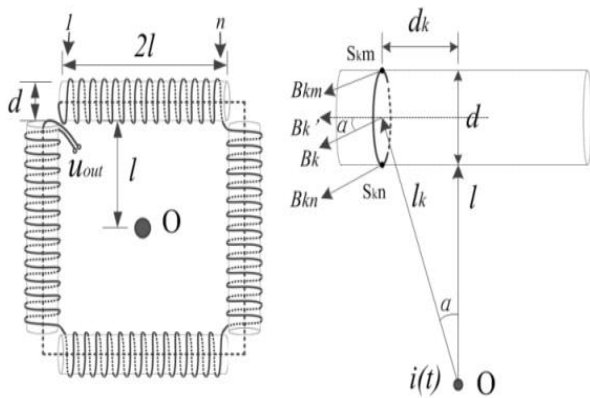
FIGURE 2. Picture of square Rogowski coils.

FIGURE 3. Diagram of square Rogowski coil.

FIGURE 4. Schematic diagram of position influence.

direction of the Rogowski coil is:

$$B_k' = \mu_r \mu_0 * \frac{i(t)}{2\pi * l_k} * \frac{l + d/2}{l_k} \qquad (3)$$

The magnetic flux is:

$$\phi_k = \oint B_k' dS = \mu_r \mu_0 * \frac{(l + d/2)d^2}{8l_k^2} * i(t) \qquad (4)$$

Where,

$$l_k^2 = l^2 + \left(\frac{2l * (\frac{N}{2} - k)}{N}\right)^2 = 2l^2 * \frac{N^2 - 2Nk + 2k^2}{N^2} \qquad (5)$$

The corresponding magnetic chain is:

$$\begin{aligned}\phi &= \sum_{k=1}^{N} \varphi_k \\ &= \frac{\mu_r \mu_0 d^2 N^2 * i(t)}{16(l + \frac{d}{2})} * \sum_{k=1}^{N} \frac{1}{N^2 - 2Nk + 2k^2}\end{aligned} \qquad (6)$$

The output voltage of the four coils is

$$\begin{aligned}u_{out} &= -4 * \frac{d\phi}{dt} \\ &= -\frac{\mu_r \mu_0 d^2 N^2}{4l} * \sum_{k=1}^{N} \frac{1}{N^2 - 2Nk + 2k^2} * \frac{di(t)}{dt}\end{aligned} \qquad (7)$$

The parameters of the designed Rogowski coil are as follows: primary rated current is 600A, $d = 5mm$, $N = 412$coil turns, $l = 21mm$, the output voltage $u_{out} = 60.52mV$. A analog integrator is used to restore the waveform.

The ideal location of Rogowski coil is that the primary conductor located at the center of the Rogowski coil, and perpendicular to the coil plane (Fig.4a), but there is always a positional deviation when installed, such as angle inclining (Fig.4b), center position offsetting (Fig.4c), vertical interference from adjacent conductor (Fig.4d), and parallel interference from adjacent conductor (Fig.4e). Suppose the mutual inductance coefficient is M when the conductor is in an ideal position, and the mutual inductance coefficient is M' when the conductor offsets. The relative error between M and M' is $\Delta l = \frac{M' - M}{M} \times 100\%$.

Simulation results are shown in Fig.5.

Fig.5a, 5b, 5c and 5d show the ratio errors of different position influences shown in Fig.4b, 4c, 4d, 4e, respectively. From Fig.5 we can see that the mutual inductance of square Rogowski coil is closely related to the position deviation and

large dynamic range, wide measurement band, no magnetic saturation and so on [33]–[35]. This system uses a square structure Rogowski coil as the current sensor, and the square structure is easy to manufacture. Many coil turns can be gotten in a small size, and is easy to be installed in the OLTC. As is shown in Fig.2, the basic structure of a square Rogowski coil contains 4 straight rods with winding coils. The detailed calculation model is established in this paper, as shown in Fig.3.

The magnetic induction intensity of the internal side of *kth* coil is as follows:

$$B_{kn} = \mu_r \mu_0 H_{kn} = \mu_r \mu_0 * \frac{i(t)}{2\pi * \sqrt{l^2 + d_k^2}} \qquad (1)$$

The magnetic induction intensity of the external side is:

$$B_{km} = \mu_r \mu_0 H_{km} = \mu_r \mu_0 * \frac{i(t)}{2\pi * \sqrt{(l + d)^2 + d_k^2}} \qquad (2)$$

Where, μ_r is the relative permeability, μ_0 is the vacuum permeability, i(t) is the AC current of point O. When $l > 8d$, and then $B_{kn}/B_{km} < 1.008$, so the magnetic field of the cross-section can be thought as equal everywhere approximately. The magnetic induction intensity perpendicular to the
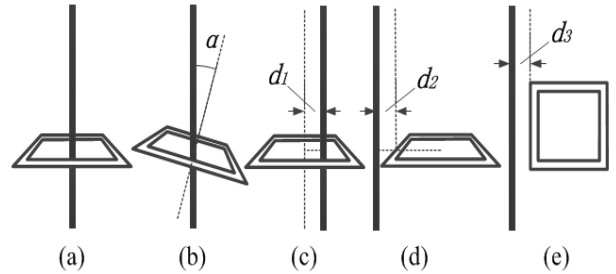
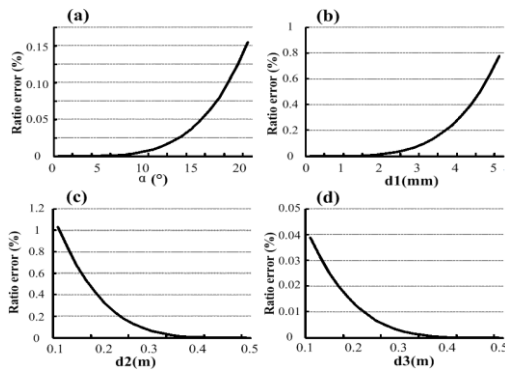| Magnetic parameters	Nanocrystalline	Permalloy 1J85	Silicon steelsheets
Saturation induction intensity (Bs/T)	1.25	0.76	2.03
Initial permeability(Gs/Oe)	40 000~80 000	50 000~80 000	1000
Maximum permeability (Gs/Oe)	>200 000	>200 000	40 000
Core lamination factor	>0.70	0.9	0.95

FIGURE 5. Simulation results of position influence.

FIGURE 6. Power supply circuit diagram.

the influence of adjacent conductor. In the actual installation, the signal acquisition system is fixed to reduce the influence of position deviation, and the distance between adjacent conductors is generally larger than 0.3m, so the measurement error can be guaranteed to be less than 0.1% by improving the manufacturing process and fixing installation.

B. DESIGN OF POWER SUPPLY CIRCUIT FOR THE SIGNAL ACQUISITION SYSTEM

The power supply to the signal acquisition circuit of high voltage side is a key technique. Commonly used power supply methods are laser energy, primary voltage energy, and primary current energy. The laser energy acquisition device has a complex structure and high price, and its long-term operation reliability and stability need to be improved. The circuit of power supply method from primary voltage is also complex, and the grounding and insulation technologies should be considered. As a result, the power supply method from primary current is adopted, which has a simple and reliable circuit.

Only one conductor has current at the same time, line 1 or line 2. Therefore, the power supply module should gather the energy from CT I and CT II simultaneously. The design of power supply circuit contains two parts: design of CT and energy acquisition circuit.

The commonly used ferromagnetic materials include nanocrystalline, permalloy, and silicon steel sheet. It can be seen from Table 1 that the nanocrystalline has high permeability, and can obtain more energy when the current is small. Its saturation magnetic induction intensity is higher than that of permalloy, and its core lamination factor is small. So small capacity and light weight can be achieved. Therefore, the nanocrystalline is used as the iron core of CT.
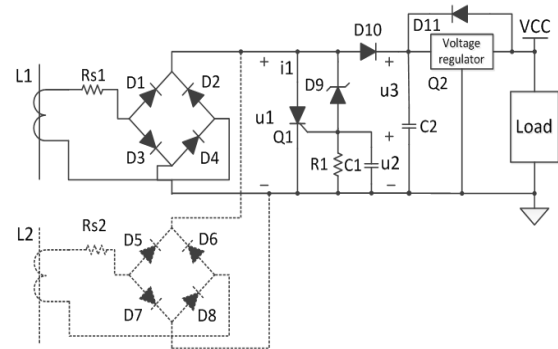
When the energy coil is working in the linear area, the secondary output power is

$$P_2 = E_2 I_2 = 4.44 f S K_p B I_1 \qquad (8)$$

Where S is the iron core sectional area, B is the magnetic flux density, I1 is the primary current, Kp is the core lamination factor with a value of 0.8, f is the frequency with a value of 50Hz. I2 is the secondary current, and E2 is the secondary output voltage.

By using a low power single chip and an efficient fiber-optical sender, the power consumption of the signal conversion circuit is very low with a value of 35mW. Consider a certain remainder, the design output power P2 is 100mW, E2 = 5V, I2 = 20mA. When the starting current I1 is 20A, the core will be saturated and then the value of B is 1.25. So the iron core sectional area of nanocrystalline is 22.5mm2 by using the above formulas. The coil turns N = 1000.

The schematic diagram of primary current complementary power supply circuit is shown in Fig. 6. Taking phase A as the example. L1 and L2 are the energy acquisition CTs in line A1 and A2, Rs1 and Rs2are internal resistances of the CT coil, D1 ∼ D4 and D5 ∼ D8 are the rectifier bridges. The rectified signals are connected in parallel so that the CTI and the CTII can be complementary to each other. Q1 is a thyristor, D9 is a 5.5V voltage regulator tube. D9, R1 and C1 form the trigger circuit. When the voltage u2 is higher than the trigger voltage of Q1, Q1 will be turned on, and the current flows through Q1 to absorb excess energy. C2 is an energy storage capacitor. The energy storage capacitor can supply the circuit when circuit I and II cannot provide normal energy supply in a short term during the process of switching. Q2 is a three terminal regulator, and the output voltage is 3.3V.

C. ALGORITHM DESIGN

As the fault current waveforms contain rich transient signal, and is non-stationary signal. So the traditional analysis methods such as FFT transform and wavelet transform are commonly used for stationary or piecewise stationary signal. FFT cannot analyze the instantaneous spectrum of the fault current waveform, and wavelet transform cannot be adaptive. Due to the finite length of wavelet basis function, energy leakage will be gathered in waveform analysis, and quantitative analysis of the energy-frequency-time relationship is difficult. The time-frequency spectrum of the switching process waveform can be established by HHT, and the local characteristics of handover waveform can be highlighted, and also has the advantages of adaptive decomposition, so it is suitable for dynamic signal analysis in the handover process.

The EMD-HHT transform includes Empirical Mode Decomposition (EMD) and Hilbert-Huang Transform (HHT). Firstly, the signal is adaptively decomposed into a series of intrinsic mode function (IMF) according to the characteristics by EMD, and the essential characteristics can be extracted. And then, each IMF is transformed by HHT, and the Hilbert-Huang spectrum is obtained to characterize the relationship among time, frequency and amplitude. For an arbitrary signal x(t), the basic processes of the EMD decomposition are as follows:

(1) Find all the maximum and minimum points of x(t), and get the upper and lower envelopes of x(t) by using curve fitting.

(2) Let m(t) be the average value of the upper and lower envelopes, and h(t) = x(t)-m(t). h(t)can be regarded as an IMF approximately.

(3) Let h(t) as a new x(t), repeat step (1) and (2) until h(t) satisfies the IMF condition. And then the first order IMF can be obtained and recorded as c1(t).

(4) Let r(t) = x(t)-c1(t) as a new x(t), repeat step (1), (2) and (3). And then the second order IMF, third order IMF, ..., at last, we can get:

$$x(t) = \sum_{k=1}^{n} c_k(t) + r(t) \qquad (9)$$

Where r(t) is the residual function and represents the average trend of the signal.

(5) By using HHT for each IMF in formula (8) we can get

$$x(t) = Re \sum_{k=1}^{n} a_k(t) e^{j\theta(t)}$$
$$= Re \sum_{k=1}^{n} a_k(t) e^{j \int \omega_k(t)dt} \qquad (10)$$

In formula (10), the residual function r(t) is neglected, and Re is used to represent the real part. Formula (9) is known as Hilbert spectrum and recorded as:

$$H(\omega, t) = Re \sum_{k=1}^{n} a_k(t) e^{j \int \omega_k(t)dt} \qquad (11)$$

Analysis was carried out to multi-components nonlinear signals by using EMD-HHT time-frequency analysis and
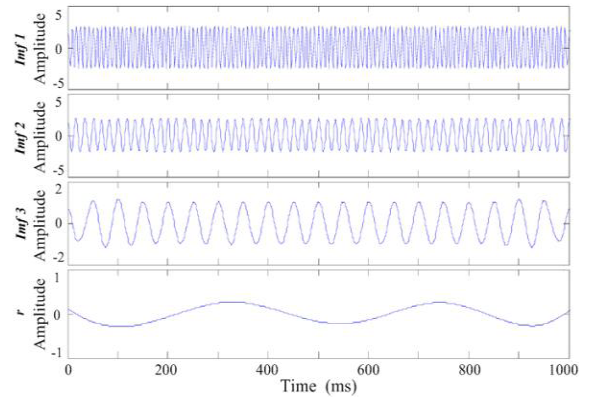
FIGURE 7. EMD decomposition diagram.

wavelet analysis method. The signals are as follows:

$$s(t) = \cos(40\pi t) + 2\cos(120\pi t + 0.5\sin 30\pi t)$$
$$+ 2.5\cos(240\pi t) \qquad (12)$$

Firstly, the EMD analysis method is used to decompose the maximum frequency component, as shown in Fig.7. *Imf1* represents the signal component of 120Hz, *Imf2* represents the signal component of 60Hz with a frequency modulation components of 15Hz, *Imf3* represents the signal component of 20Hz. r is the residual quantity. The Hilbert time-frequency spectrum of the original signal can be obtained by HHT analysis of the IMF component, as shown in Fig.8.

From Fig.8a we can see that the wavelet transform can distinguish the frequency components of 20Hz and 120Hz, while the result is not good for the signal component of 60Hz with frequency modulation components of 15Hz. In Fig.8a, the frequency changes with time are not clearly shown for the signal component of 60Hz. As the given frequency modulation signal is 2cos(120πt+0.5sin30πt), the fluctuation range of the frequency is 52.5 Hz to 67.5 Hz. Fig.8b clearly shows this feature. Therefore, the spectrum diagram can be clearly obtained by HHT in Fig.8b. The dynamic characteristic of frequency varying with time, and the component of frequency modulation is also very clear. The results show that the HHT time-frequency analysis is more suitable for capturing the current characteristic of the switching process and making the fault feature diagnosis.

IV. PERFORMANCE TEST

In order to verify that the signal acquisition system can accurately collect the fault signal, basic accuracy test and transient performance test were carried out, and then, the fault diagnosis performance of the system was verified in the factory area.

A. BASIC ACCURACY TEST

The experiment is to verify the accuracy of square Rogowski coil by compared with a standard current transformer (HLS-47A), which has high accuracy of 0.02 classes. The test platform is realized by using a NI 24-bits data acquisition
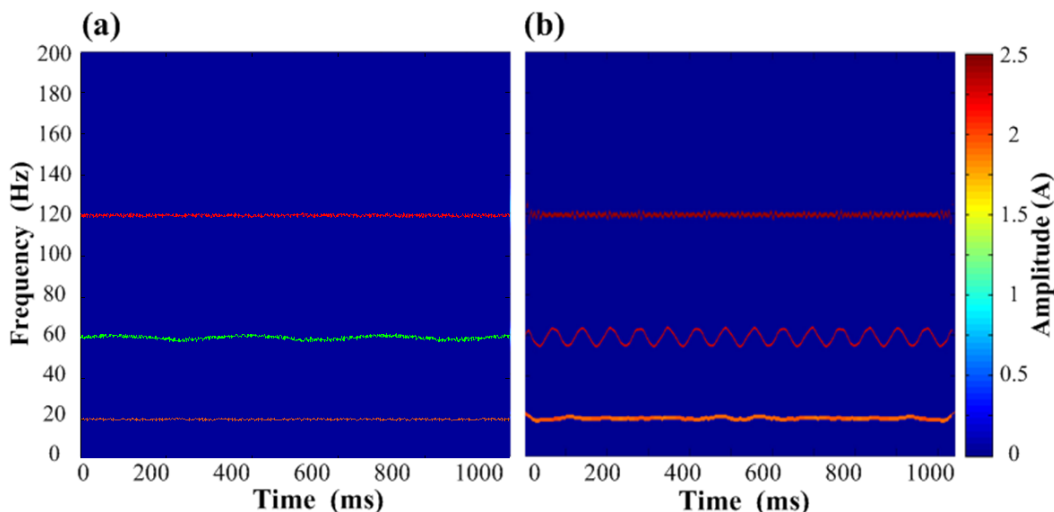
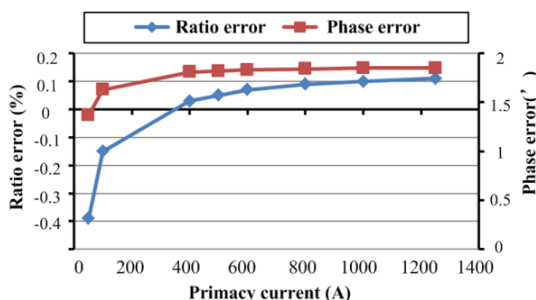**FIGURE 8. Normalized spectrum of wavelet and HHT transform.**

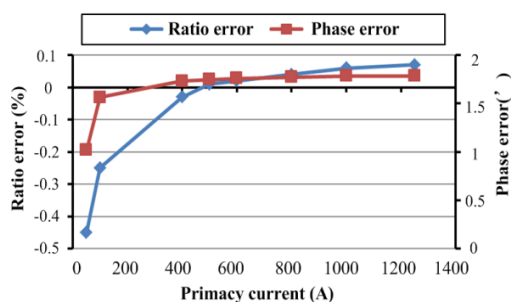**FIGURE 9. Measurement error of the master sensor.**

FIGURE 10. Measurement error of the secondary sensor

card. The rated current of the square Rogowski coil is 600A. When the current changes to 12A ~ 1200A, the error between the standard transformer and the Rogowski coil is shown in Fig.9 and Fig.10.

The test results show that the maximum ratio error is less than 0.45% and the phase error is less than 2' in the range of 12 to 1200A.

B. TRANSIENT PERFORMANCE ERROR TEST
In order to verify the transient performance of the system, the response experiment of transient large current was

TABLE 2. Transient measurement error of the designed system.

	time constant/ms	short-circuit current/A	peak current/A
shunt	62	516	1483
current sensor	60	512	1476
measuring error/%	-1.61	-0.58	-0.47

carried out. The short circuit fault of the power grid is simulated by a sudden short circuit when the AC generator is running normally, which can provide a transient current with the peak value of 20 times the normal value. A shunt (2kA:75mV) is connected in series. The output of the shunt is regarded as the standard signal, and its output voltage waveform is recorded by SL1400 ScopeCorder LITE. The data processing software of the transient test system is calculated according to the requirements of IEC 62271-100. The waveforms of the shunt and the designed current sensor and signal acquisition system are shown in Fig.11 and the waveform data is shown in Table 2.

From Fig.11 and Table 2 we can see that the transient waveform of the designed system is consistent with the shunt. The results show that the designed signal acquisition system has excellent dynamic performance, and meets the transient error requirements of IEC standard. The time delay of a system is very important [36], [37]. From table 2 we can see that the error of time constant is -1.61% and meet the requirement.

C. FAULT DIAGNOSIS TEST
The fault diagnosis of two OLTCs is presented. These OLTCs are transported to the factory for repair. Tests were carried out with the current of 400A and voltage of 10kV by using the designed on-line fault diagnosis system and the results are as follows.
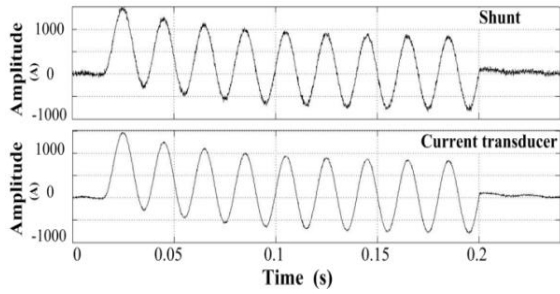
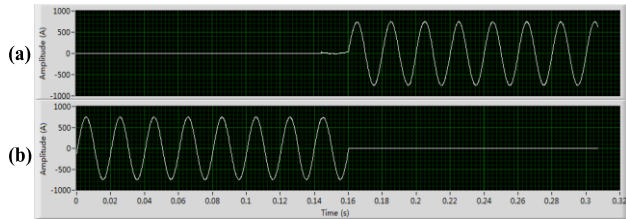**FIGURE 11.** Waveforms of transient performance error test.

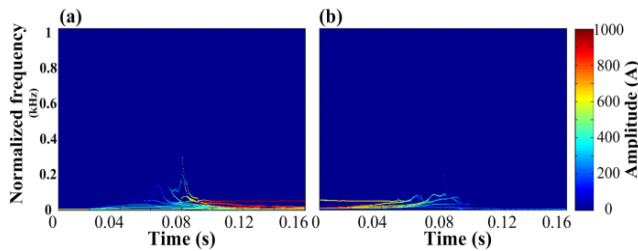**FIGURE 12.** Current waveform of switching process of normal OLTC.

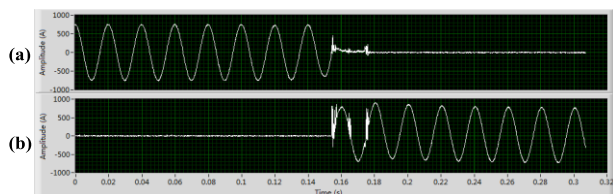**FIGURE 13.** EMD-HHT analysis of current waveform of normal OLTC.

FIGURE 14. Current waveform of switching process of failure OLTC a.

FIGURE 15. EMD-HHT analysis of current waveform of failure OLTC a.

FIGURE 16. Current waveform of switching process of failure OLTC b.

FIGURE 17. EMD-HHT analysis of current waveform of failure OLTC b.

The current waveform of the fixed contact terminal of normal OLTC in the switching process is shown in Fig.12 and Fig.13. Fig.13a is the current waveform of the odd side fixed contact by HHT analysis and Fig.13b is the waveform of even side. It can be seen from the picture that the switch is switched from the even side to the odd side at the time of 0.08s, and the current waveform is mainly composed of 50Hz component.

Fig.14 is the test waveform of the first failure OLTC a. Fig.15a is the normalized frequency time spectrum of the odd side fixed contact terminal by EMD-HHT transform and Fig.15b is the normalized spectrum of the even side fixed contact terminal. From Fig.15a and Fig.15b (1 and 2), we can see that there are rich frequency components in the waveforms. According to the analysis of fault characteristic quantities,
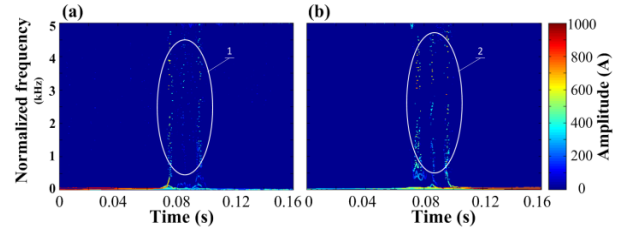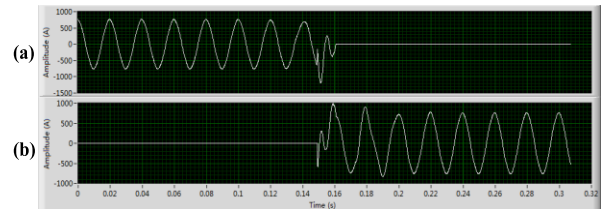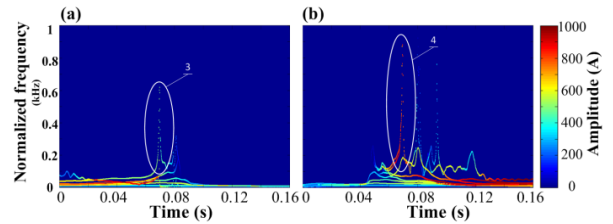
the OLTC is likely to have a fault of contact terminals, which can produce arcing in the process of switching and lead to rich frequency components.

Fig.16 is the test waveform of the failure OLTC b and Fig.17 is EMD-HHT results. It can be seen from Fig.17a that the signal contains frequency components of 50 ∼ 600Hz in the waveform of odd side contact when switching and the amplitude is larger than 400A. In Fig.17b the amplitude of the frequency components of 50 ∼ 800Hz in the even side contact is larger than 600A, and also the continuity of the power frequency component in the switching process is poor. According to the analysis, the transition resistance of OLTC b is likely to be reduced, which leads to a larger current when the resistors are connected to the circuit.

For OLTC a, we found that the fixed contact and the movable contact are obviously ablated, and the contact terminal is not smooth as usual. It will work normally after changing the fixed contact and the movable contact terminals. For OLTC b, we measured the resistance and its value is 2.1 Ω, which is less than the normal value (3.2Ω). The failure phenomenon will disappear after the transition resistance is replaced.

The test results show that the designed current sensors and fault diagnosis system can capture transient signals in the switching process accurately. Normalized frequency time spectrum can be obtained through the EMD-HHT analysis, and then the fault characteristics from the original signals can

be distinguished, so the fault of the OLTC can be effectively diagnosed.

V. CONCLUSION

To guarantee the performance of OLTC used in the power grid of aerospace engineering, a fault diagnosis method and system based on current detection in the switching process is proposed in this paper. Under the premise of ensuring good insulation, the current signals of the fixed contact are gathered by a square Rogowski coil acquisition system. An EMD-HHT algorithm is used to calculate and analyze the current waveform of the switching process and extract the fault feature to diagnose the fault sources in the fault diagnosis software. Experiments show that the current sensor and signal acquisition system can collect the dynamic current waveform in the switching process, and capture the high frequency components of fault signals. The software is used to analyze the current waveform through EMD-HHT algorithm. The system can accurately identify the fault events of OLTC, and make effective fault diagnosis. The system can provide theoretical basis for the condition maintenance of OLTC, and detect early faults in time. It can prevent the faults of OLTC from expanding, so as to ensure the safety of power systems. To further improve the system performance, new algorithms and sensors, like sliding mode technique and optical sensors will be the next research direction in future.

REFERENCES

[1] C. Roncero-Clemente and E. Roanes-Lozano, "A multi-criteria computer package for power transformer fault detection and diagnosis," *Appl. Math. Comput.*, vol. 319, pp. 153–164, Feb. 2018.

[2] Q. Gao, A. S. Kammer, U. Zalluhoglu, and N. Olgac, "Combination of sign inverting and delay scheduling control concepts for multiple-delay dynamics," *Syst. Control Lett.*, vol. 77, pp. 55–62, Mar. 2015.

[3] P. S. Georgilakis, J. A. Katsigiannis, K. P. Valavanis, and A. T. Souflaris, "A systematic stochastic Petri Net based methodology for transformer fault diagnosis and repair actions," *J. Intell. Robot. Syst.*, vol. 45, no. 2, pp. 181–201, 2006.

[4] Q. Gao, A. S. Kammer, U. Zalluhoglu, and N. Olgac, "Critical effects of the polarity change in delayed states within an LTI dynamics with multiple delays," *IEEE Trans. Autom. Control*, vol. 60, no. 11, pp. 3018–3022, Nov. 2015.

[5] Z. Wu, B. Li, C. Dang, F. Hu, Q. Zhu, and B. Fu, "Solving long haul airline disruption problem caused by groundings using a distributed fixed-point computational approach to integer programming," *Neurocomputing*, vol. 269, pp. 232–255, Dec. 2017.

[6] H. R. Karimi and H. Gao, "New delay-dependent exponential H_∞ synchronization for uncertain neural networks with mixed time delays," *IEEE Trans. Syst., Man, Cybern. B, Cybern.*, vol. 40, no. 1, pp. 173–185, Feb. 2010.

[7] L. Jae-Yoon, L. Dae-Jong, and J. Pyeong-Shik, "Fault diagnosis of oil-filled power transformer using DGA and intelligent probability model," *Trans. Korean Inst. Elect. Eng. P*, vol. 65, no. 3, pp. 188–193, 2016.

[8] J. C. Castro, G. S. Lagos, and O. A. Gonzalez, "Simulation and simulation and measuring transients in on-load tap changers," *IEEE Latin Amer. Trans.*, vol. 15, no. 10, pp. 1901–1907, Oct. 2017.

[9] Z. Wu, B. Li, and C. Dang, "Solving multiple fleet airline disruption problems using a distributed-computation approach to integer programming," *IEEE Access*, vol. 5, pp. 19116–19131, 2017.

[10] B. B. Munyazikwiye, H. R. Karimi, and K. G. Robbersmyr, "Optimization of vehicle-to-vehicle frontal crash model based on measured data using genetic algorithm," *IEEE Access*, vol. 6, pp. 3131–3138, 2017.

[11] A. Cichoń, S. Borucki, and D. Zmarzly, "Estimate of the repeatability measurement results obtained by acoustic emission method in the diagnosis of on-load tap changers," *Przeglad Elektrotechniczny*, vol. 88, no. 11, pp. 264–267, 2012.

[12] Q. Gao and N. Olgac, "Bounds of imaginary spectra of LTI systems in the domain of two of the multiple time delays," *Automatica*, vol. 72, pp. 235–241, Oct. 2016.

[13] A. Cichoń, S. Borucki, and P. Berger, "Selecting sensor for on load tap changer contacts degree of wear diagnostics," *Acta Phys. Polonica A*, vol. 124, no. 3, pp. 395–398, 2013.

[14] A. Zecchino, J. Hu, M. Marinelli, and M. Coppo, "Experimental testing and model validation of a decoupled-phase on-load tap-changer transformer in an active network," *IET Generat., Transmiss. Distrib.*, vol. 10, no. 15, pp. 3834–3843, 2016.

[15] H. R. Karimi, "A sliding mode approach to H_∞ synchronization of masterŰslave time-delay systems with Markovian jumping parameters and nonlinear uncertainties," *J. Franklin Inst.*, vol. 349, no. 4, pp. 1480–1496, 2012.

[16] Z. Wu, Q. Gao, B. Li, C. Dang, and F. Hu, "A rapid solving method to large airline disruption problems caused by airports closure," *IEEE Access*, vol. 5, pp. 26545–26555, 2017.

[17] A. Cichon, P. Fracz, and D. Zmarzly, "Characteristic of acoustic signals generated by operation of on load tap changers," *Acta Phys. Polonica A*, vol. 120, no. 4, pp. 585–588, 2011.

[18] Y. Li, H. R. Karimi, Q. Zhang, D. Zhao, and Y. Li, "Fault detection for linear discrete time-varying systems subject to random sensor delay: A Riccati equation approach," *IEEE Trans. Circuits Syst. I, Reg. Papers*, vol. 65, no. 5, pp. 1707–1716, May 2018.

[19] J. L. F. Chacon, E. A. Andicoberry, V. Kappatos, M. Papaelias, C. Selcuk, and T.-H. Gan, "An experimental study on the applicability of acoustic emission for wind turbine gearbox health diagnosis," *J. Low Freq. Noise Vibrat. Active Control*, vol. 35, no. 1, pp. 64–76, 2016.

[20] L. Gao, F. Zai, S. Su, H. Wang, P. Chen, and L. Liu, "Study and application of acoustic emission testing in fault diagnosis of low-speed heavy-duty gears," *Sensors*, vol. 11, no. 1, pp. 599–611, 2011.

[21] Y. Li, S. Liu, M. Zhong, and S. X. Ding, "State estimation for stochastic discrete-time systems with multiplicative noises and unknown inputs over fading channels," *Appl. Math. Comput.*, vol. 320, pp. 116–130, Mar. 2018.

[22] Y. Li, S. Liu, and Z. Wang, "Fault detection for linear discrete time-varying systems with intermittent observations and quantization errors," *Asian J. Control*, vol. 18, no. 1, pp. 377–389, 2016.

[23] D. Paliwal, A. Choudhury, and T. Govardhan, "Detection of bearing defects from noisy vibration signals using a coupled method of wavelet analysis followed by FFT analysis," *J. Vibrat. Eng. Technol.*, vol. 5, no. 1, pp. 21–34, 2017.

[24] R. Yan and R. X. Gao, "Hilbert–Huang transform-based vibration signal analysis for machine health monitoring," *IEEE Trans. Instrum. Meas.*, vol. 55, no. 6, pp. 2320–2329, Dec. 2006.

[25] W. Fan, X. Wang, L. Wang, and Z. Yu, "The application of Hilbert–Huang transform energy spectrum in brushless direct current motor vibration signals monitoring of unmanned aerial vehicle," *Adv. Mech. Eng.*, vol. 8, no. 9, pp. 1–7, 2016.

[26] Y. Wang, H. Shen, H. R. Karimi, and D. Duan, "Dissipativity-based fuzzy integral sliding mode control of continuous-time T-S fuzzy systems," *IEEE Trans. Fuzzy Syst.*, Jun. 2017, doi: 10.1109/TFUZZ.2017.2710952.

[27] Y. Wang, Y. Xia, H. Shen, and P. Zhou, "SMC design for robust stabilization of nonlinear Markovian jump singular systems," *IEEE Trans. Autom. Control*, vol. 63, no. 1, pp. 219–224, Jan. 2018.

[28] J. Liu, G. Wang, L. Zhang, and T. Zhao, "Fault diagnosis of on-load tap-changer based on variational mode decomposition and relevance vector machine," *Energies*, vol. 10, no. 7, p. 946, 2017.

[29] R. Duan and F. Wang, "Fault diagnosis of on-load tap-changer in converter transformer based on time–frequency vibration analysis," *IEEE Trans. Ind. Electron.*, vol. 63, no. 6, pp. 3815–3824, Jun. 2016.

[30] S. Szkolka and G. Wisniewski, "Unconventional small power voltage transformer," *Przeglad Elektrotechniczny*, vol. 8, no. 85, pp. 123–126, 2009.

[31] T. A. Mellik, T. J. Dionise, and R. Yanniello, "A case study of voltage transformer failures: Solution implementation in a modern data center," *IEEE Ind. Appl. Mag.*, vol. 24, no. 1, pp. 98–109, Jan.-Feb. 2018.

[32] M. Tajdinian, M. Allahbakhshi, A. Bagheri, and A. R. Seifi, "Analytical discrete Fourier transformer-based phasor estimation method for reducing transient impact of capacitor voltage transformer," *IET Generat., Transmiss. Distrib.*, vol. 11, no. 9, pp. 2324–2332, 2017.

[33] Z.-H. Li, S.-H. Yan, Z.-X. Li, Y.-C. Xu, and W.-Z. Hu, "High accuracy on-line calibration system for current transformers based on clamp-shape Rogowski coil and improved digital integrator," *Mapan-J. Metrol. Soc. India*, vol. 31, no. 2, pp. 119–127, 2016.

[34] I. A. Metwally, "Tape-wound Rogowski coil for measuring large-magnitude pulsed currents," *J. Instrum. Experim. Techn.*, vol. 59, no. 2, pp. 250–257, Mar. 2016.

[35] T. Tao, Z. Zhao, W. Ma, Q. Pan, and A. Hu, "Design of PCB Rogowski coil and analysis of anti-interference property," *IEEE Trans. Electromagn. Compat.*, vol. 58, no. 2, pp. 344–355, Apr. 2016.

[36] Q. Gao and N. Olgac, "Stability analysis for LTI systems with multiple time delays using the bounds of its imaginary spectra," *Syst. Control Lett.*, vol. 102, pp. 112–118, Apr. 2017.

[37] Q. Gao, U. Zalluhoglu, and N. Olgac, "Investigation of local stability transitions in the spectral delay space and delay space," *ASME J. Dyn. Syst., Meas. Control*, vol. 136, no. 5, p. 051011, 2014.

ZHENGTIAN WU received the B.Sc. degree in mechanical manufacturing and automation from the Hefei University of Technology, China, in 2008, and the two Ph.D. degrees in operations research from the University of Science and Technology of China and the City University of Hong Kong in 2014. He is currently a Lecture with the Suzhou University of Science and Technology, Suzhou, China. His research interests include Nash equilibrium, mixed integer programming, approximation algorithm, and distributed computation.

ZHENHUA LI received the B.Sc. degree in biotechnology and the Ph.D. degree in electric engineering from the Huazhong University of Science and Technology, China, in 2008 and 2014, respectively. He is currently an Associate Professor with China Three Gorges University, Yichang, China. His research interests include condition monitoring of aircraft electric power source, electromagnetic compatibility, energy measurement, approximation algorithm, and fault diagnosis.

QIUHUI LI received the B.Sc. degree in electrical engineering and automation from the College of Science and technology, China Three Gorges University, Yichang, China, in 2016, where she is currently pursuing the master's degree. Her research interests include condition monitoring of power grid, electromagnetic compatibility, and fault diagnosis.
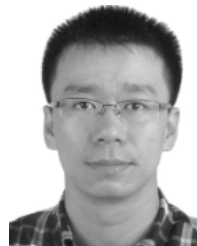
JIE YU received the B.Sc. degree in electrical engineering and automation from Linyi University, China, in 2015. She is currently pursuing the master's degree with China Three Gorges University, Yichang, China. Her research interests include condition monitoring of power transformer, electromagnetic compatibility, and fault diagnosis.

RONGHAO ZHENG received the bachelor's degree in electrical engineering and the master's degree in control theory and control engineering from Zhejiang University, China, in 2007 and 2010, respectively, and the Ph.D. degree in mechanical and biomedical engineering from the City University of Hong Kong in 2014. He is currently an Associate Professor with the College of Electrical Engineering, Zhejiang University. His research interests lie in the area of distributed algorithms and control, especially the coordination of networked mobile robot teams with applications in automated systems and security.

• • •